CrossMark

Single/Dual Fano Resonance Based on Plasmonic Metal-Dielectric-Metal Waveguide

Kunhua Wen[1] · Yihua Hu[1] · Li Chen[1] · Jinyun Zhou[1] · Liang Lei[1] · Ziming Meng[1]

Abstract A plasmonic metal-dielectric-metal (MDM) waveguide structure is proposed by placing a slot cavity below or above a groove. The groove and the slot cavity can act as a reflector and a resonator, respectively. Due to the interactions between the broad dark mode and the narrow bright mode caused by the groove and the side-coupled slot cavity, single Fano resonance with sharp asymmetric spectral profile is achieved. Interestingly, dual Fano resonances can also be obtained by using two different slot cavities, which are simultaneously distributed on both sides of the groove. The line shape can be transformed by changing the length of the groove, while the wavelength of the resonance peak can be manipulated linearly with the length of the slot cavity. The proposed structure yields a highest sensitivity of ~1131 nm/RIU and a figure of merit of ~1.6×10^7, and thus, we believe that it can serve as an on-chip nanosensor.

Introduction

Recently, Fano resonance has attracted considerable attention in the field of plasmonics due to its unique characteristics. Unlike the conventional symmetric resonant Lorentzian line profile, the spectrum based on Fano resonance possesses an asymmetric one, which can provide high figure of merit (FOM) and sensitivity. Such a resonance phenomena is firstly discovered in the auto-ionizing states of atoms [1], and then is also found in the classical optical systems.

By taking advantage of surface plasmon polaritons (SPPs) which can overcome the classical optical diffraction limit, on-chip Fano resonance can be achieved in various plasmonic structures, showing great potential in the sensors, switching, nonlinear, and slow-light areas [2–6]. Specifically, the asymmetric spectral response can be obtained through the interference between a localized dark mode (corresponding to the discrete excited state) and a radiative bright mode (corresponding to the continuum state). For example, Fano resonance was observed in a dolmen-type slab structure consisting of a radiative element and a sub-radiant element [7]. Besides, plasmon rulers [8], core-shell structures [9], plasmonic nanoparticle clusters [10], composite cut-wire structures [11], planar plasmonic structure [12], and other structures [13–15] have been investigated theoretically or experimentally to obtain Fano-like resonances. It is worth to point out that plasmonic metal-dielectric-metal (MDM) waveguide structures have also received a lot of interest in studying Fano resonance due to the advantages of high integration, deep-subwavelength confinement of light, and easily manufactured [16–20]. Sharp and asymmetric Fano-line shapes were found in an MDM waveguide with multiple output ports, which were isolated by the baffles [21]. More and more MDM structures were developed to realize the Fano resonances, such as wide-gap and narrow-gap hybrid MDM structure [22], one-terminal-closed T-shaped MDM structure [23], and so on. In addition, a MDM bus waveguide with dual side-coupled slot cavities or dual parallel grooves were proposed to obtain the asymmetric spectrum with high sensitivity and FOM [24, 25]. According to demands of nanosensors, the FOM was further improved by employing an MDM T-shaped resonator [26].

✉ Kunhua Wen
   wkh2003@gmail.com

[1] School of Physics and Optoelectronic Engineering, Guangdong University of Technology, Guangzhou 510006, Guangdong, China

In this paper, single or dual Fano resonance peaks are achieved by using a compact MIM waveguide structure, which is a composite of slot cavities and grooves. Since the slot cavities and the grooves can act as the Fabry-Perot (FP) resonators and the reflectors, thus bright modes with narrow bands and dark modes with broad bands are excited, respectively. Due to the interactions of the bright and dark modes, Fano resonances will then be generated. The spectral line profile and the peak wavelength can be manipulated by changing the lengths of the grooves and the slot cavities, respectively. The structure presents a high refractive index sensitivity and a FOM higher than the previous reported results.

Theory and Analysis

Figure 1 shows the scheme diagram of the plasmonic MDM waveguide structure. A groove is placed on one side of the MDM waveguide, while a side-coupled slot cavity is laid on the opposite side with a coupling distance d. When SPPs are launched into the MDM waveguide, they will be captured into the slot cavities and then oscillated around the groove, which is analogous to the classical Fano resonances of mechanical spring harmonic oscillator system [27]. Besides, the Fano-like resonance phenomenon can also be explained by the coherent coupling and interference between the bright mode and the dark mode. Since the slot cavity can act as a FP resonator, a narrow bright mode can be achieved at the wavelength, expressed as

$$\lambda = \frac{2n_s L}{m - \phi / 2\pi}, \quad m = 1, 2, 3, \cdots \quad (1)$$

where L is the length of the slot cavity, ϕ is the phase change due to the reflection at the FP facet, and m is an integer. n_s is the real part of the effective index, which can be obtained from the dispersion equation [28]. Moreover, a broad dark mode will be exited by the groove due to the equivalent Bragg reflection. Due to the interaction of two modes, Fano resonance is generated to obtain a distinctly asymmetrical spectral profile, which is completely different from the Lorentzian resonance. The line shape of the transmission spectrum will be affected by the groove, while the wavelength of the Fano peak

Fig. 1 Scheme diagram of the plasmonic MDM waveguide structure

will be determined by the length of the slot cavity, as shown in Eq. (1). The sensitivity S and FOM, which are the two significantly factors to evaluate the performances, can be expressed as [29, 30]

$$S = \frac{d\lambda}{dn(\lambda)} \quad (2)$$

$$FOM^* = \left| \frac{dT(\lambda) / dn(\lambda)}{T(\lambda)} \right| \quad (3)$$

$$FOM = Max(FOM^*) \quad (4)$$

where $T(\lambda)$ is the transmittance at the specific wavelength, and $dT(\lambda)/dn(\lambda)$ is the transmittance change at fixed wavelength induced by a refractive index change. Based on Eqs. (3) and (4), it can be predicted that an ultra-low transmittance and a sharp increase of the transmittance induced by the index changes are preferred for obtaining a high FOM.

In the following, 2D FDTD simulation with perfect matched layer is used to investigate the performances, and the grid sizes are set to be 5 nm×5 nm. PML layers with reflection of 0.0001 are set to surround the whole structure, and the fundamental TM mode of the plasmonic waveguide is excited by a plane wave incident from the input waveguide. The dielectric and metal are assumed to be air and silver, whose optical constant is obtained from the experiment [28]. The width and length of the slot cavity are defined as $W_3=50$ nm and $L=360$ nm, respectively. The coupling distances from the slot cavity to the MDM bus waveguide is $d=25$ nm, the length of the groove is $H=200$ nm, and the widths of the MDM waveguide and the groove are $W_1=50$ nm and $W_2=130$ nm, respectively. To better understand the modes excited by the groove and the slot cavity, we firstly consider the MDM structure only with the groove or the slot cavity, respectively. When the MDM waveguide is only with the groove, the transmission spectrum is shown in Fig. 2 with a blue solid line. A broadband transmission dip with a negligible transmittance (low than −50 dB) arises at the wavelength of ~970 nm. In contrast, the structure only with the slot cavity presents a much narrower transmission at the wavelength of ~1179 nm with a slight higher transmittance (~0.04), as shown in Fig. 2 with a red dot. When the MDM structure is with both the groove and the slot cavity, obviously, asymmetric Fano resonance peak is achieved at ~1187 nm with a transmittance of ~0.5 according to the modes interactions, as shown in Fig. 2 with a black dotted line. Besides, the quality factor (QF) of the Fano resonance is ~18.

Secondly, the length of the groove is changed as $H=290$ nm to find more characteristics. The transmission spectrum is shown in Fig. 3, where asymmetrical spectral profiles are also achieved due to the Fano resonance effect. Comparing to the results in Fig. 2, the spectral profile presents an obvious
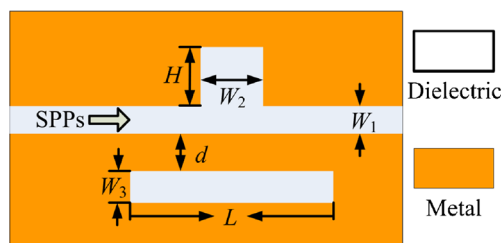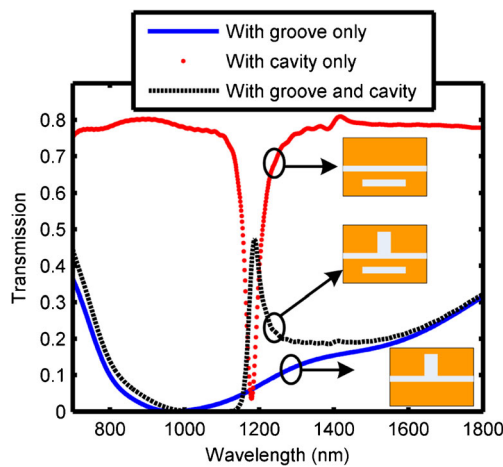
Fig. 2 Transmission spectra with groove only (*blue solid line*), or with cavity only (*red dotted*), or with groove and slot cavity (*black dotted line*)

transformation by changing H. The reversal mechanism of the asymmetric spectral profile can be attributed to the shift of the broad dark mode, which is determined by length H of the groove. For example, the right rising edge of the broad dark mode will interact with the narrow bright mode firstly. When the length of the groove is increased, the dark mode has a red shift and then its left rising edge will affect the resonance. In Fig. 3, a sharp transmission peak with a transmittance of ~0.5 and a QF of ~22 arises at 1170 nm, and the transmittance will decrease rapidly at the right side of the peak, resulting in a transmission dip with an ultra-low transmittance. Similar results are also obtained in Fig. 2 except for the dip, which emerges at the left side of the peak. Therefore, the line shape can be manipulated by changing the length of the groove.

Figure 4 provides the magnetic field distributions of SPPs at the Fano peak wavelengths and the dip wavelengths that correspond to the results in Figs. 2 and 3. Specifically, SPPs at the peak wavelengths of 1170 and 1187 nm in Fig. 4a, c, respectively, can pass through the MDM waveguide. Strong field distributions are observed in the slot cavity that acts as a FP resonator, leading to a narrow transmission peak.
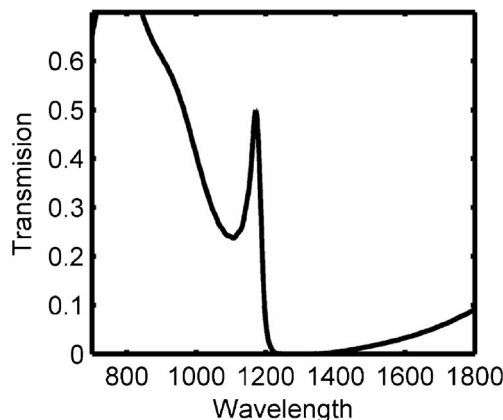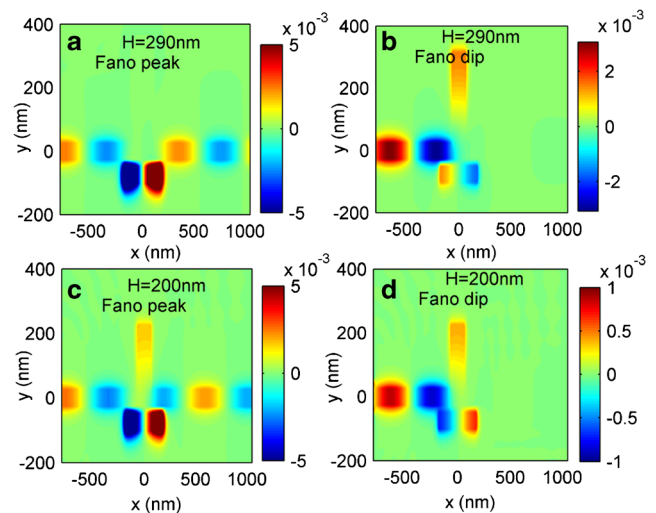

Fig. 4 Magnetic field distributions of SPPs at the peak wavelengths and the dip wavelengths that correspond to the results in Figs. 2 and 3: **a** $\lambda=$ 1170 nm, **b** $\lambda=1252$ nm, **c** $\lambda=1187$ nm, and **d** $\lambda=1106$ nm

Conversely, SPPs at the dip wavelengths (i.e., 1252 nm in Fig. 4b and 1106 nm in Fig. 4d) show a weak distribution in the slot cavity but a strong one in the groove, and thus, most of the SPPs are blocked by the groove. Due to the interaction of the narrow discrete bright mode (strong trapped resonance in the FP resonator) and the broad dark mode (strong reflection in the groove), sharp and asymmetric spectra, which are regarded as Fano resonances, can be obtained. These straightforward results in Fig. 4 provide the SPP power flows in our proposed structure in detail.

According to Eq. (1), the peak wavelength should have a linear relationship with the length of the slot cavity. The analysis results are further confirmed by FDTD simulations, as shown in Fig. 5. By fixing the length of the groove as 200 or 290 nm and the dielectric as air, we firstly increase the length of the slot cavity from 330 to 380 nm with a step of 10 nm. Obviously, an average slope of the increasing peak wavelength is obtained as 2.89 and 2.91 by fixing $H=200$ and 290 nm, respectively, as shown in the left side of Fig. 5
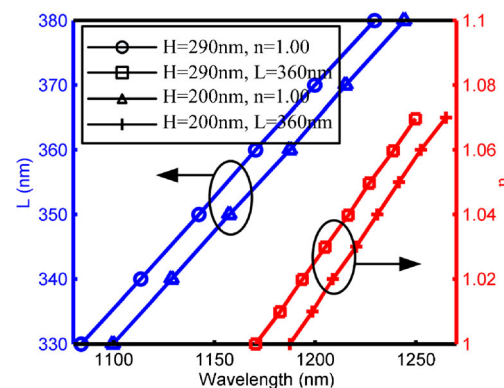

Fig. 3 Transmission spectra with $H=290$ nm

Fig. 5 The variations of peak wavelengths with respect to the length of the slot cavity and the refractive index of the dielectric

with blue lines. Then, one can easily manipulate the wavelength by adjusting the length of the slot cavity. Besides, a linear relationship between the wavelength and the refractive index of the dielectric is also investigated by fixing the lengths of the groove and the slot cavity. The details are presented by using the red line in the right side of Fig. 5, where the refractive index of the dielectric is increased from 1 to 1.07 with a step of 0.01. As a result, the sensitivity of the structure can be calculated as 1106 and 1131 nm/RIU with $H=200$ and 290 nm, respectively. This is also the desired character for the sensors, which require a high sensitivity.

To better evaluate the performance of the proposed structure, the FOM is also studied in detail. Based on Eqs. (3) and (4), FOM* corresponding to the case in Figs. 2 and 3 (i.e., $H=$ 200, 290 nm) is shown in Fig. 6 by changing the refractive index of the dielectric. The values of FOM are as high as 5.0×10^4 and 1.6×10^7 at 1251 and 1164 nm in Fig. 6a, b, respectively. These FOM values are significantly greater than that in the previous reports [22–26]. Due to this outstanding property, we consider that the proposed structure can work as a sensor well.

In the next step, the slot cavity is proposed to be laid above the groove, as shown in Fig. 7. In this case, SPPs will propagate into groove and then be captured into the slot cavity, which is different from that in Fig. 1. However, the oscillation around the groove for SPPs will still occur. This phenomenon is also analogous to mechanical spring, while the slot cavity performs as the fixed end of the spring. Since the slot cavity and the groove will still provide a narrow dark mode and a broad bright mode, respectively, Fano resonance should be generated via the modes interaction. By setting the length of the groove as $L=560$ nm, the coupling distance $d=30$ nm, and other parameters to be unchanged, FDTD simulations are used to investigate the performances. The transmission spectra and the FOM* are shown in Fig. 8 by defining $H=200$ and 150 nm.

Obviously, Fano resonances are observed in Fig. 8a, b, which show the sharp and asymmetrical peaks at 888 and 1187 nm with the QFs of ~68 and ~72, respectively. Comparing to the results in Fig. 2, the transmission peaks possess smaller full width at half-maximums for the reason that the second-order resonance mode of the slot cavity is used. In
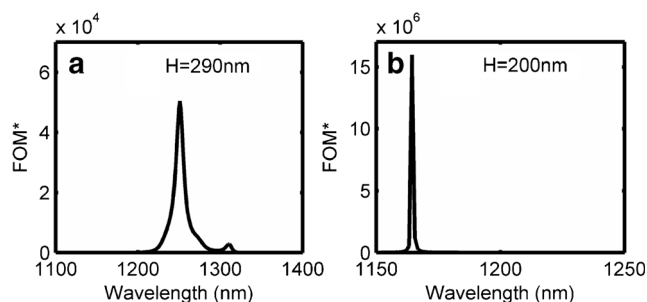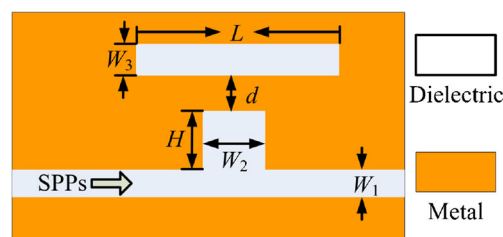

Fig. 7 The MDM waveguide structure with different slot cavity arrangement

Fig. 8a with $H=200$ nm, a steep slope emerges at the left side of the Fano peak, resulting in a dip with ultra-low transmittance. By changing the parameter H to be 150 nm, the transmittance decreases rapidly from the peak wavelength to the long wavelength, and then a transmission dip arises at the right side of peak. According to the FOM* plotted with a red dotted line, a large FOM of 5.0×10^4 or 2.3×10^4 is achieved at the dip with the wavelength of 871 or 900 nm in Fig. 8a, b, respectively.

More details about the magnetic field distributions are provided in Fig. 9. Specifically, Fig. 9a, c are the SPP propagation details at the Fano peaks with the wavelengths of 887 and 883 nm, while Fig. 9b, d are field distributions at the Fano dips with the wavelengths of 871 and 883 nm, respectively. Obviously, most of the SPPs at the peak wavelengths can pass through the MDM waveguide, but those at the dip wavelengths are almost completely stopped by the groove. The results agree well with those in Fig. 8.

The variations of the peak wavelengths with respect to the length L of the slot cavity or the refractive index n of the dielectric are shown in Fig. 10. By increasing L from 520 to 600 nm with a step of 10 nm, we can obtain a uniform increase step of the wavelength as ~13.4 nm with $H=150$ and 200 nm. Likewise, a linear relationship between the wavelengths and n is also confirmed, and then a sensitivity of 840 and 847.5 nm/ RIU is investigated with $H=150$ and 200 nm, respectively.

According to the spectral line profiles in Figs. 2, 3, and 7, it is investigated that a Fano peak at the expected wavelength can be achieved by laying the slot cavity below or above the groove. It is interesting to explore more performances by
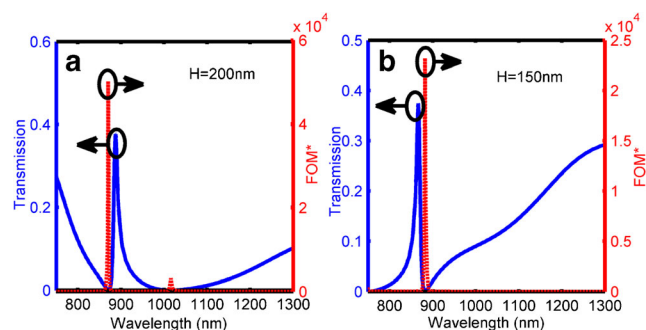

Fig. 6 The calculated FOM* corresponding to Figs. 2 and 3

Fig. 8 The transmission spectra and the FOM* with **a** $H=200$ nm and **b** $H=150$ nm
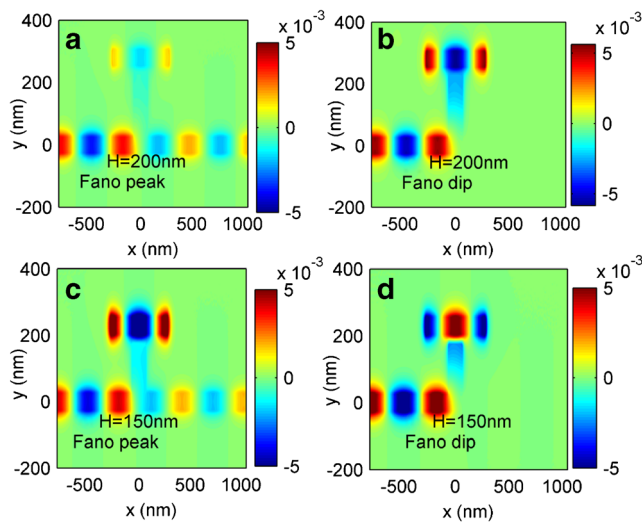
Fig. 9 Magnetic field distributions of SPPs at the peak wavelengths and the dip wavelengths that correspond to the results in Fig. 8: **a** λ=887 nm, **b** λ=871 nm, **c** λ=883 nm, and **d** λ=900 nm

Fig. 11 The MDM waveguide structure with two slot cavities

adding two slot cavities in the structure, as shown in Fig. 11. According to the resonance conditions, two slot cavities with different lengths should support two specific bright modes. These two modes will be interacted with the dark mode from the groove, respectively, and actually, the two interaction processes are immune to each other because of the different wavelengths of the bight modes. As a result, dual Fano peak should be available in the new proposed structure. To perform the FDTD simulation, all the parameters are defined as L_1= 560 nm, d_1=30 nm, L_2=360 nm, d_2=25 nm, H=200 nm, W_1=W_3=50 nm, and W_2=130 nm.

Figure 12 shows the transmission spectrum, where two Fano peaks with the QFs of ~61 and ~35 arise at the wavelengths of 888 and 1187 nm, respectively. The steep slopes appear at the left sides of the peaks, resulting in the dips with ultra-low transmittances. These results are completely identical to the results in Figs. 2 and 8a, and the spectral profile seems to be their perfect synthesis because of the same
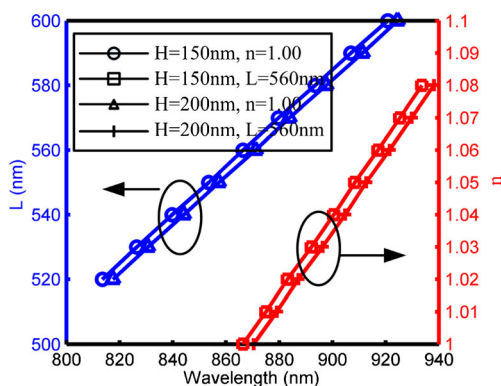
parameters. This phenomenon is attributed to the independent interactions between the broad mode from the groove and the two narrow modes from two slot cavities, respectively. The FOM* are also provided in Fig. 12, where a large FOM of 2.2×10^4 and 2.9×10^4 is achieved at 873 and 1138 nm, respectively. Consequently, one can obtain dual Fano resonance peaks with comparable performances by using this composite structure. The magnetic field distributions of SPPs are also provided in Fig. 13, where sub-graphs (a) and (c) correspond to the peak wavelengths of 888 and 1187 nm, and sub-graphs (b) and (d) are the dip wavelengths of 873 and 1138 nm, respectively. The simulations are similar to that in Figs. 4 and 9, where most of the SPPs at the peak wavelengths can pass through the MDM waveguide while those at the dip wavelengths will be stopped.

Furthermore, the length of one slot cavity is changed while another one is fixed to find out more characters of the structure. Firstly, L_2=360 nm and L_1= 560, 580, and 600 nm are employed in Fig. 14a–c. Obviously, the wavelength of the left Fano peak has a linear red shift along with the linear increase of L_1, but the right Fano peak always stays at the identical wavelength due to the same value of L_2. Likewise, the right Fano Peak increase linear proportionally with L_2 in Fig. 14c– e, where L_2 is defined from 360 to 400 nm with a step of 20 nm. Besides, the wavelength of left Fano peak is

Fig. 10 The variations of peak wavelengths with respect to the length of the slot cavity and the refractive index of the dielectric

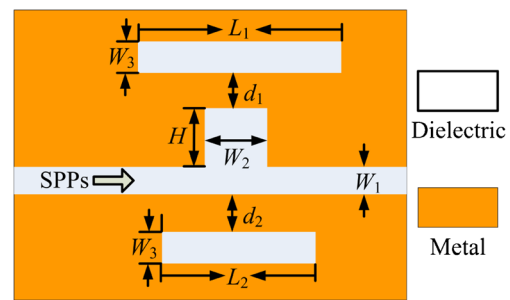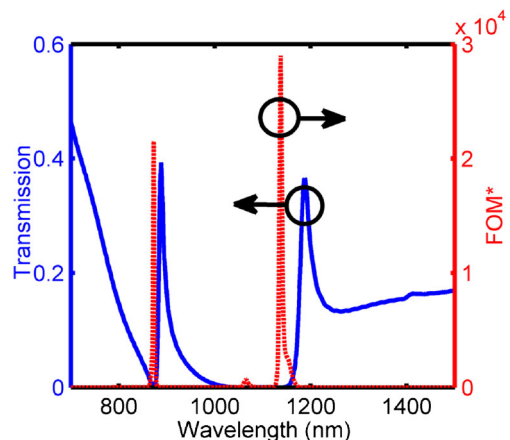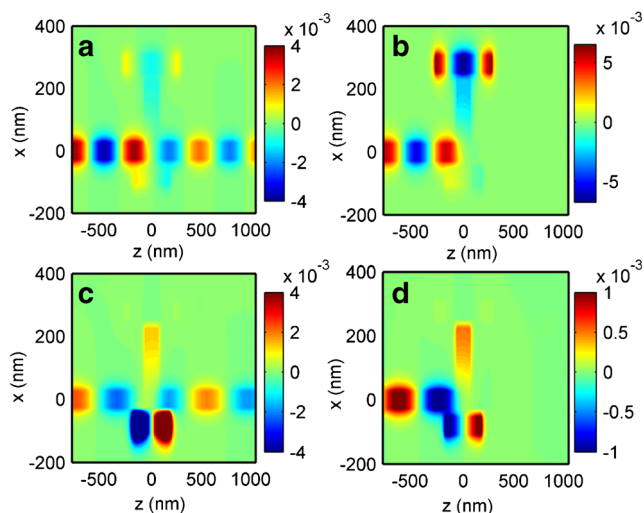**Fig. 12** The transmission spectra and the FOM* of the composite structure

Fig. 13 Magnetic field distributions of SPPs at the peak wavelengths and the dip wavelengths of **a** $\lambda=888$ nm, **b** $\lambda=873$ nm, **c** $\lambda=1187$ nm, and **d** $\lambda=1138$ nm

unchanged due to the same L_1 of 600 nm. Based on the simulations, the variations of the peak wavelengths with respect to the lengths of the cavities are further investigated. Therefore, one can easily design the specific Fano peak at the expected wavelength by changing the corresponding slot cavity but without any influence on the other peak. This character may offer great flexibility to design the device.
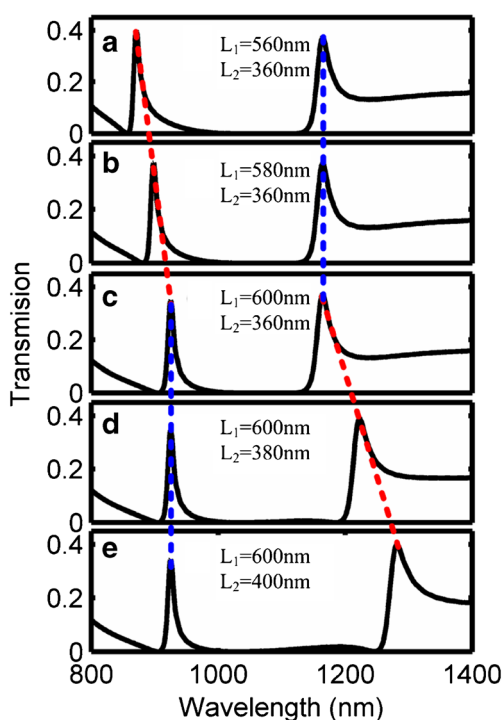

Fig. 14 The transmission spectra with **a** $L_1=560$ nm, $L_2=360$ nm, **b** $L_1=580$ nm, $L_2=360$ nm, **c** $L_1=600$ nm, $L_2=360$ nm, **d** $L_1=600$ nm, $L_2=380$ nm, and **e** $L_1=600$ nm, $L_2=400$ nm

Conclusion

In summary, Fano resonances have been investigated in our proposed MDM structure. According to the interactions between the narrow bright modes provided by the slot cavities and the broad dark mode from the groove, asymmetric line shapes were achieved. Single or dual Fano peaks, whose wavelengths were determined by the lengths of the slot cavities, could be obtained by designing the arrangements of the slot cavities. Besides, the line shape could be transformed by changing the length of the groove. The device could serve as an on-chip nanosensor due to the highest sensitivity and FOM as 1131 nm/RIU and 1.6×10^7, respectively.

Compliance with Ethical Standards This research does not involve in any human participant or animal. No part of this manuscript has been published or submitted elsewhere. Also, all the authors have given their approvals to the submission of this paper.

Conflict of Interest The authors declare that they have no conflict of interests.

References

1. Fano U (1961) Effects of configuration interaction on intensities and phase shifts. Phys Rev 124(6):1866–1878
2. Verellen N, Sonnefraud Y, Sobhani H, Hao F, Moshchalkov VV, Van Dorpe P, Nordlander P, Maier SA (2009) Fano resonances in individual coherent plasmonic nanocavities. Nano Lett 9(4):1663–1667
3. Miroshnichenko E, Flach S, Kivshar YS (2010) Fano resonances in nanoscale structures. Rev Mod Phys 82(3):2257–2298
4. Luk'yanchuk B, Zheludev NI, Maier SA, Halas NJ, Nordlander P, Giessen H, Chong CT (2010) The Fano resonance in plasmonic nanostructures and metamaterials. Nature Mater 9(9):707–715
5. Zhang ZD, Wang HY, Zhang ZY (2013) Fano resonance in a gear-shaped nanocavity of the metal-insulator-metal waveguide. Plasmonics 8(2):797–801
6. Miroshnichenko AE, Kivshar YS (2005) Engineering Fano resonances in discrete arrays. Phys Rev E 72(5):056611
7. Zhang S, Genov DA, Wang Y, Liu M, Zhang X (2008) Plasmon-induced transparency in metamaterials. Phys Rev Lett 101(4):047401
8. Liu N, Hentschel M, Weiss T, Alivisatos AP, Giessen H (2011) Three-dimensional plasmon rulers. Science 332(6036):1407–1410
9. Hu Y, Noelck SJ, Drezek RA (2010) Symmetry breaking in gold-silica-gold multilayer nanoshells. ACS Nano 4(3):1521–1528

10. Fan JA, Wu C, Bao K, Bao J, Bardhan R, Halas NJ, Manoharan VN, Nordlander P, Shvets G, Capasso F (2010) Self-assembled plasmonic nanoparticle clusters. Science 328(5982):1135–1138

11. Artar A, Yanik AA, Altug H (2011) Directional double Fano resonances in plasmonic hetero-oligomers. Nano Lett 11(9):3694–3700

12. Wang JQ, Fan CZ, He JN, Ding P, Liang EJ, Xue QZ (2013) Double Fano resonances due to interplay of electric and magnetic plasmon modes in planar plasmonic structure with high sensing sensitivity. Opt Express 21(2):2236–2244

13. Zhang ZS, Yang ZJ, Li JB, Hao ZH, Wang QQ (2011) Plasmonic interferences in two-dimensional stacked double-disk array. Appl Phys Lett 98(17):173111

14. Fang ZY, Cai J, Yan Z, Nordlander P, Halas NJ, Zhu X (2011) Removing a wedge from a metallic nanodisk reveals a Fano resonance. Nano Lett 11(10):4475–4479

15. Zhang S, Bao K, Halas NJ, Xu H, Nordlander P (2011) Substrate-induced Fano resonances of a plasmonic nanocube: a route to increased-sensitivity localized surface plasmon resonance sensors revealed. Nano Lett 11(4):1657–1663

16. Wen KH, Yan LS, Hu YH, Chen L, Lei L (2014) A plasmonic wavelength-selected intersection structure. Plasmonics 9(3):685–690

17. Wen KH, Yan LS, Pan W, Luo B, Guo Z, Guo YH, Luo XG (2014) Electromagnetically induced transparency-like transmission in a compact side-coupled T-shaped resonator. J Lightwave Technol 32(9):1701–1707

18. Song G, Yu L, Wu C, Duan G, Wang L, Xiao J (2013) Polarization splitter with optical bistability in metal gap waveguide nanocavities. Plasmonics 8(2):943–947

19. Liu Y, Zhou F, Yao B, Cao J, Mao Q (2013) High-extinction-ratio and low-insertion-loss plasmonic filter with coherent coupled nano-cavity array in a MIM waveguide. Plasmonics 8(2):1035–1041

20. Qi J, Chen Z, Chen J, Li Y, Qiang W, Xu J, Sun Q (2014) Independently tunable double Fano resonances in asymmetric MIM waveguide structure. Opt Express 22(12):14688–14695

21. Chen J, Li Z, Li J, Gong Q (2011) Compact and high-resolution plasmonic wavelength demultiplexers based on Fano interference. Opt Express 19(10):9976–9985

22. Chen Z, Chen JJ, Yu L, Xiao JH (2015) Sharp trapped resonances by exciting the anti-symmetric waveguide mode in a metal-insulator-metal resonator. Plasmonics 10(1):131–137

23. Shang XJ, Li XF, Wang LL, Zhai X, Lin Q, Wang BX, Li Q (2015) Realizing Fano-like resonance in a one terminal closed T-shaped waveguide. European Phys J B 88(6):1–5

24. Chen J, Li Z, Zou Y, Deng Z, Xiao J, Gong Q (2013) Coupled-resonator-induced Fano resonances for plasmonic sensing with ultra-high figure of merits. Plasmonics 8(4):1627–1631

25. Lu H, Liu X, Mao D, Wang G (2012) Plasmonic nanosensor based on Fano resonance in waveguide-coupled resonators. Opt Lett 37(18):3780–3782

26. Wen KH, Hu YH, Chen L, Zhou JY, Lei L, Guo Z (2015) Fano resonance with ultra-high figure of merits based on plasmonic metal-insulator-metal waveguide. Plasmonics 10(1):27–32

27. Joe YS, Satanin AM, Kim CS (2006) Classical analogy of Fano resonances. Phys Scrip 74(2):259–266

28. Johnson PB, Christy RW (1972) Optical constants of the noble metals. Phys Rev B 6(12):4370–4379

29. Becker J, Trügler A, Jakab A, Hohenester U, Sönnichsen C (2010) The optimal aspect ratio of gold nanorods for plasmonic bio-sensing. Plasmonics 5(2):161–167

30. Ameling R, Langguth L, Hentsche M, Mesch M, Braun PV, Giessen H (2010) Cavity-enhanced localized plasmon resonance sensing. Appl Phys Lett 97(25):253116